

# Improving power system stability in the presence of wind farms using STATCOM and predictive control strategy

Mohsen Darabian<sup>1</sup>, Abolfazl Jalilvand<sup>1</sup> ✉

<sup>1</sup>Department of Electrical Engineering, University of Zanjan, Zanjan, Iran

✉ E-mail: m.darabian@znu.ac.ir

ISSN 1752-1416

Received on 23rd September 2016

Revised 13th June 2017

Accepted on 6th October 2017

E-First on 16th November 2017

doi: 10.1049/iet-rpg.2016.0812

www.ietdl.org

**Abstract:** In this study, a multi-objective predictive control strategy is presented for the stability improvement of a power system in the presence of wind farms and STATCOM. The main contribution of this study is in the multi-objective consideration for controlling the active and reactive powers of the rotor-side converter in each of the induction generators, controlling the voltage of the synchronous generators' excitation system, and designing the damping controller of STATCOM using the predictive strategy. To reduce the computational burden, and to accurately choose the input paths into the predictive control, the Laguerre functions are used. Also, for reducing the sampling time in the selection of large prediction horizons, the exponential data weighting has been employed. The simulation results were evaluated using MATLAB software in the field of time and frequency under different scenarios. Moreover, the obtained results of each domain are compared using the two techniques of the predictive strategy, i.e. the classic model, Laguerre functions, and also the conventional proportional integral controller. The comparison of these three methods reveals that the functional predictive control outfits the two other controllers in damping of the oscillations.

## Nomenclature

$P_{ot}$	extracted power from the wind turbine (watts)	$P_{rw}$	active power of the rotor-side converter
$\rho_{ot}$	air density ( $\text{kg/m}^3$ )	$P_{gw}$	active power of the grid-side converter
$K_{ot}$	swept area of blades ( $\text{m}^2$ )	$C_{dc}$	capacity of the DC link capacitor
$V_{ot}$	wind speed (m/s);	$V_{dc}$	voltage of the DC link capacitor
$D_{ot}$	performance coefficient of blades	$Z_{q1} \ \& \ Z_{i1}$	PI controller coefficients for regulating the reactive power
$\beta_{ot}$	blade pitch angle	$Z_{q2} \ \& \ Z_{i2}$	PI controller coefficients for regulating the current of RSC
$\lambda_{ot}$	tip speed ratio	$Z_{q3} \ \& \ Z_{i3}$	PI controller coefficients for regulating the speed of RSC
$d_1 - d_9$	constants	$i_{drw\_ref}$	current control in $d$ -axis for RSC
$R_b$	blade radius (m)	$i_{qrw\_ref}$	current control in $q$ -axis for RSC
$\omega_b$	angular velocity of the blade (rad/s)	$Q_{sw\_ref}$	reference reactive power
$L_{ss}$	self-inductance of stator	$\omega_{rw\_ref}$	reference speed
$L_{rr}$	self-inductance of rotor	$Z_{bg} \ \& \ Z_{ig}$	coefficients of the PI controller for regulating the voltage of DC link capacitor
$L_{mm}$	mutual inductance	$Z_{pb} \ \& \ Z_{pi}$	coefficients of the PI controller for regulating the current of GSC
$R_s$	stator resistance	$i_{qgw\_ref}$	reference current control in $q$ -axis for GSC
$R_r$	rotor resistance	$V_{dc\_ref}$	reference voltage of the DC link capacitor
$i_{ds}$	stator current in $d$ -axis	$Z_{b\beta} \ \& \ Z_{i\beta}$	coefficients of the PI controller;
$i_{qs}$	stator current in $q$ -axis	$\tau_{b\beta}$	delay time constant for blade pitch angle control
$i_{dr}$	rotor current in $d$ -axis	$P_{gw}$	power of wind turbine measured for the blade pitch angle control
$v_{ds}$	stator voltage in $d$ -axis	$P_{gw\_ref}$	reference power of wind turbine for the blade pitch angle control
$v_{dr}$	rotor voltage in $d$ -axis	$\mathbf{x}(z)$	state vector of MPC
$v_{qs}$	stator voltage in $q$ -axis	$\mathbf{b}(z)$	input vector of MPC
$v_{dr}$	rotor voltage in $d$ -axis	$\mathbf{c}(z)$	disturbance vector of MPC
$v_{qr}$	rotor voltage in $q$ -axis	$\mathbf{k}(z)$	output vector of MPC
$H_t$	inertia constant of wind turbine	$z$	sampling time of MPC
$H_g$	inertia constant of generator	$\mathbf{G}_z$	weighting matrix of the cost function
$\omega_t$	angular speed of the wind turbine	$\mathbf{S}_z$	weighting matrix of control action in the cost function
$\omega_r$	angular speed of the rotor of the generator	$\mathbf{k}'(r+z)$	prediction vector of the output signal
$T_{ot}$	mechanical torque of wind turbine	$\mathbf{k}_{ref}(r+z)$	reference path of system's future
$T_{tg}$	shaft torque	$\Delta\mathbf{b}(r+z)$	action control vector
$T_{eot}$	electrical torque of wind turbine		
$K_t$	damping coefficient of turbine		
$K_g$	damping coefficient of generator		
$K_{tg}$	inertia constant of wind turbine		
$L_{tg}$	inertia constant of generator		
$P_{dc}$	active power of the DC link		

## 1 Introduction

Recently, variable-speed constant-frequency generators are usually utilised in the wind turbines; among these generators, the doubly fed induction generators (DFIGs) and permanent magnet ones are more prevalent [1, 2]. To prevent the undesirable effects of a wind turbine outage, all the new installed turbines must be able to pass through the fault condition, i.e. they must remain connected in the case of fault occurrence and limited voltage drop in PCC. The utilisation of FACTS devices plays an important role in compensating this voltage drop, and hence, they contribute to the power system stability [3].

The use of superconducting magnetic energy storage (SMES) and STATCOM both can be applied as parallel compensators to improve the dynamic stability of the power system in the presence of wind farms [4, 5]. Hence, artificial intelligence-based algorithms are used in [4, 5] to design FACTS devices' controllers in order to acquire a proper dynamic response. A neural network-based adaptive technique and shuffled frog-leaping algorithms are employed in [4, 5] to design the controllers for SMES and STATCOM, respectively. In these two references, the wind farm is considered just as a simple induction generator, not as a DFIG. Therefore no control action is used on rotor side and grid side converters.

In the power system, every fault, even when cleared, brings about some oscillations; these oscillations are the so-called low-frequency oscillations (LFOs). In this regard, the design of damping controllers will be very useful for the series or parallel compensators. If the controllers are properly designed, they will be able to sufficiently increase the power system stability [6–8]. For this aim, Ref. [6] has addressed the design of damping controllers for the static VAR compensator (SVC) in order to improve the voltage drop resulted from the fault occurrence in a single-machine power system connected to an infinite bus in the presence of wind farms. The utilised method for the design of SVC controllers was based on an adaptive neural fuzzy network. In a similar way, the researches in [7, 8] have designed the controllers of STATCOM in the single-machine and multi-machine power systems, respectively. It is worth mentioning that the controllers are only designed for the FACTS devices, and no controller has been considered for the converters of the wind farms. To achieve an acceptable range of stability in a power system, in addition to the use of FACTS devices, it is required to optimally adjust the controllers of the grid-side converters (GSCs) and rotor-side converters (RSCs). One of the techniques used for reducing the LFOs in DFIGs is to put a feedback control on the active and reactive powers of the converter. The input of this control loop, which is named power system stabiliser (PSS), is the power flowing through the line [9]. The main idea of this work is the application of PSS to the induction generator and tuning its parameters using the fuzzy system. A wide-area damping controller design is employed in [10] to mitigate LFOs. The shaft torsional oscillation, as well as destabilising the wind turbine generator system operation may also occur as a result of employing these control strategies which are not taken into account in the above-mentioned studies.

A heuristic dynamic programming (HDP) is employed in [11] to control the reactive power of a large-scale wind farm along with a STATCOM in a coordinated manner. The performance of the DFIG can be enhanced using HDP in the case of fault occurrence in the grid. The main drawback of this strategy is the need for pre-training in order to be connected to the grid. Ref. [12] addresses the relation between rotor angles and DFIG reactive power control in a large-scale power system. The large rotor angle swings can be diminished by reducing reactive power absorbed by DFIGs, and consequently, the reactive power injection by the synchronous generators is also mitigated.

The model predictive control (MPC) is one of the efficient control strategies, which is considered by a wide range of research studies in electrical engineering. This strategy has several advantages such as its simplicity and high control accuracy. Consequently, the MPC has been employed for adjusting the control signals of PSS [13] and high voltage direct current (HVDC) system [14] in order to damp the LFOs. A HVDC supplementary

controller design based on the discrete-time MPC is described in [15] to alleviate the oscillatory modes of two-power systems. WSCC and IEEE 14-bus power systems are used for a single-loop and meshed cases, respectively. A comparison study is also made between the proposed MPC technique and a linear quadratic Gaussian technique in terms of damping effects. In addition, a line-commutated current-sourced converter-based HVDC system is considered to apply the proposed method.

In [16], the coordinated design of the wind turbine and energy storage units has been implemented on a micro-grid using the predictive control. The aim of this work is to control the active and reactive powers of the wind turbine regarding the wind speed and load demand. It should be noticed that in this condition, the predictive control concentrates on the switching operations of the inverters in batteries and wind turbine. A variety of predictive control strategies have been proposed in the literature which all of them are based on the model [17–19]. The non-linear MPC with offset-free feature for the SVC design [17], the robust control for designing of the FACTS controllers [18], distributed MPC [19], and functional predictive control [20, 21] are some of the methods each employed for a specific purpose in the power system.

In this study, a predictive strategy is utilised for controlling the active and reactive powers of the DFIG-based wind turbine and also, for controlling the input voltage of the synchronous generators' excitation system in order to enhance the power system stability. In addition, a parallel compensator has been applied to generate the required reactive power of the wind farm and to reduce the power system oscillations. The control procedure in the compensator is in a way that the output power of the wind farm is employed as an input signal. In this way, in addition to the design of damping controller of the STATCOM, the oscillations of the power injected by the wind farm into the grid will be controlled.

The innovations of this paper can be summarised as the following:

- Active power control of the inter-area by applying an additional damping signal to the STATCOM controller in the presence of time delay.
- Active and reactive power control of a RSC in the presence of different uncertainties.
- Using logger functions in MPC to reduce the computational burden and improve the damping characteristics of the power system.

In the second section, the general modelling of the power system including the dynamic equations of the synchronous generator, induction generator, and related controllers, and also, the mathematical relations of the static compensator are comprehensively extracted. In the third section, the predictive strategy will be described by equations. The simulation results are presented in the fourth section, and finally, the last section concludes the paper.

## 2 Configuration of the system model

### 2.1 Model of the synchronous generators

In this section, the two-axis model and IEEE-DC1A exciter are employed, respectively, for analysing the dynamic model of a synchronous generator. In the two-axis model, the sub-transient effects have been disregarded, but, the transient effects of the synchronous generator are regarded by  $X'_d$  and  $X'_q$ . For the complete list of the electrical and mechanical equations of the synchronous generators, the readers are referred to Ref. [22]. In addition, the differential equations of the  $i$ th generator can be represented as

$$\frac{dE'_{qi}}{dt} = \frac{1}{T'_{doi}} [-E'_{qi} + E_{fdi} + (X_{di} - X'_{di})I_{di}] \quad (1)$$

$$\frac{dE'_{di}}{dt} = \frac{1}{T'_{qoi}} [-E'_{di} - (X_{qi} - X'_{qi})I_{qi}] \quad (2)$$



$$\begin{cases} \frac{di_{dsw}}{dt} = \omega_{base}(L_{mm}^2 - L_{ss}L_{rr})^{-1}[R_sL_{rr}i_{dsw} + ((\omega_s - \omega_r)L_{mm}^2 - \omega_sL_{rr}L_{ss})i_{qsw} - R_rL_{mm}i_{drw} - \omega_rL_{rr}L_{mm}i_{grw} + L_{mm}V_{drw} - L_{rr}V_{dsw}] \\ \frac{di_{qsw}}{dt} = \omega_{base}(L_{mm}^2 - L_{ss}L_{rr})^{-1}[(-\omega_s - \omega_r)L_{mm}^2 + \omega_sL_{rr}L_{ss}]i_{dsw} + R_sL_{rr}i_{qsw} + \omega_rL_{rr}L_{mm}i_{drw} - R_rL_{mm}i_{grw} + L_{mm}V_{grw} - L_{rr}V_{qsw}] \\ \frac{di_{drw}}{dt} = \omega_{base}(L_{mm}^2 - L_{ss}L_{rr})^{-1}[-R_sL_{mm}i_{dsw} + \omega_rL_{ss}L_{mm}i_{qsw} + R_rL_{ss}i_{drw} + (\omega_sL_{mm}^2 - (\omega_s - \omega_r)L_{ss}L_{rr})i_{grw} - L_{ss}V_{drw} + L_{mm}V_{dsw}] \\ \frac{di_{grw}}{dt} = \omega_{base}(L_{mm}^2 - L_{ss}L_{rr})^{-1}[-\omega_rL_{ss}L_{mm}i_{dsw} - R_sL_{mm}i_{qsw} + (-\omega_sL_{mm}^2 + (\omega_s - \omega_r)L_{ss}L_{rr})i_{drw} + R_rL_{ss}i_{grw} - L_{ss}V_{grw} + L_{mm}V_{qsw}] \end{cases} \quad (9)$$

$$\begin{aligned} \frac{di_{ds}}{dt} &= -\frac{\omega_s R_s}{X_s}i_{ds} + \omega_s i_{qs} - \frac{\omega_s}{X_s}\sin(\phi_b + \beta_s)V_{dc} + \frac{\omega_s}{X_s}V_{bus}\cos(\beta_s) \\ \frac{di_{qs}}{dt} &= -\omega_s i_{ds} - \frac{\omega_s R_s}{X_s}i_{qs} - \omega_s i_{qs} + \frac{\omega_s}{X_s}\cos(\phi_b + \beta_s)V_{dc} + \frac{\omega_s}{X_s}V_{bus}\sin(\beta_s) \\ \frac{dV_{dcs}}{dt} &= -\sqrt{3}\omega_s X_{dc}\sin(\phi_b + \beta_s)i_{ds} - \sqrt{3}\omega_s X_{dc}\cos(\phi_b + \beta_s)i_{qs} \end{aligned} \quad (11)$$

controllers joined together through two back-to-back voltage sources using a DC link.

In general, the mechanical power of a variable-speed wind turbine is expressed as [4, 23]

$$P_{\omega t} = \frac{1}{2}\rho_{\omega t}K_{\omega t}V_{\omega t}^3D_{\omega t}(\lambda_{\omega t}, \beta_{\omega t}) \quad (5)$$

In (5),  $D_{\omega t}$  is the efficiency coefficient which is obtained as

$$D_{\omega t}(\Phi_S, \beta_{\omega t}) = d_1\left(\frac{d_2}{\Phi_S} - d_3\beta_{\omega t} - d_4 \cdot \beta_{\omega t}^{d_5} - d_6\right)\exp\left(\frac{-d_7}{\Phi_S}\right) \quad (6)$$

Based on (6), the relations (7) and (8) can be extracted as

$$\Phi^{-1} = \left([\lambda_{\omega t} + d_8\beta_{\omega t}]^{-1} - [d_9(\beta_{\omega t}^3 + 1)^{-1}]\right) \quad (7)$$

$$\lambda_{\omega t} = (R_b\omega_b)(V_{\omega t}^3)^{-1} \quad (8)$$

### 2.3 Mathematical expression of the RSC

In this part, for the design and control of the rotor and GSCs, the vector technique has been used [24]. The control block diagram of the controllers of the RSC has been depicted in Fig. 1B. As shown, the  $q$  and  $d$  axes of the current auxiliary signal are employed for controlling of the active and reactive powers, respectively.

The mathematical equations governing the control of the RSC can be stated as (see (9))

### 2.4 Mathematical model of the STATCOM

To design the damping controller for the static compensator, its mathematical model should be determined. According to Fig. 1A, in this model, a resistance  $R_c$ , which is in parallel with a capacitor  $C$ , is utilised. This resistance represents the total switching power loss of the inverter and capacitor [7]. The output voltage of this compensator can be expressed as the following equations in the  $d$ - $q$  reference frame:

$$\begin{cases} v_{ds} = V_{dc\_s}k_{ns}\sin(\phi_b + \beta_s) \\ v_{qs} = V_{dc\_s}k_{ns}\cos(\phi_b + \beta_s) \end{cases} \quad (10)$$

In (10),  $k_{ns}$  is the modulation index,  $\beta_s$  is the phase angle of the compensator, and  $\phi_b$  is the phase angle for the voltage of the common AC bus.

Moreover, the dynamic equations related to STATCOM could be expressed in the form of a synchronous reference as [3] (see (11)) In Fig. 1C, the control block diagram for the static compensator has been given. As shown, the control of DC and AC bus's voltages is done, respectively, by  $\beta_s$  and  $k_{ns}$ . Also, the delay

operator is as an exponential function described by a first-order Pade approximation [25].

Damping control equation could be expressed as follows:

$$\frac{d\beta_s}{dt} = \frac{1}{T_I}[K_I(V_{bus}^* - V_{bus} - V_{Is}) - \beta_s] \quad (12)$$

### 3 Predictive control

In the problems requiring the prediction of system's future behaviour, the model-based predictive control is a powerful technique [26, 27]. The information predicted by this method is used to obtain the optimal point based on the criteria of each specific problem. As the basis of this method is on the process model, therefore, the predicted inputs and outputs can also be used for state estimation of the process. The new measurements of the process model sampled in each time instant are injected into the control loop, and on this basis, the predictive horizon is forecasted. The merit of this strategy is that in each sampling interval, a constrained optimisation problem is solved. The limitations and every change in the process constraints can be applied to the system as the error signal. One of the appealing features of the predictive control which has distinguished it from the other control methods is that a series of control variables with a given length, i.e. the predictive horizon is calculated for the future behaviour of the system. Fig. 2A shows the block diagram of this control method. Based on this figure, the problem constraints, the objective function, and the output of the prediction system can be applied to the optimisation system in order to obtain an appropriate output for the system. As in this paper the predictive control strategy in the multi-objective form is used, therefore, the utilised model is in the state space to accurately follow the desired objectives. Thus, the equation of the model-based predictive control is represented in the state space as:

$$\begin{cases} \mathbf{x}(z+1) = F_k\mathbf{x}(z) + G_k\mathbf{b}(z) + H_k\mathbf{c}(z) \\ \mathbf{k}(z) = P_k\mathbf{x}(z) \end{cases} \quad (13)$$

The objective function is selected in a way that the future outputs are able to track the reference signal in the prediction horizon, and the required control action is low as much as possible. To attain the desired objectives, the objective function of the predictive control can be described as: (see (14)) where the prediction vector, which is considered for the system's output, is defined as a  $1 \times m_a$  matrix in which  $m_a$  is called the prediction horizon. Also,  $\Delta\mathbf{b}$  is a  $1 \times m_b$  matrix in which  $m_b$  is named the control horizon.

#### 3.1 Considered constraints in the MPC

The following constraints are considered in solving of the problem by the predictive control:

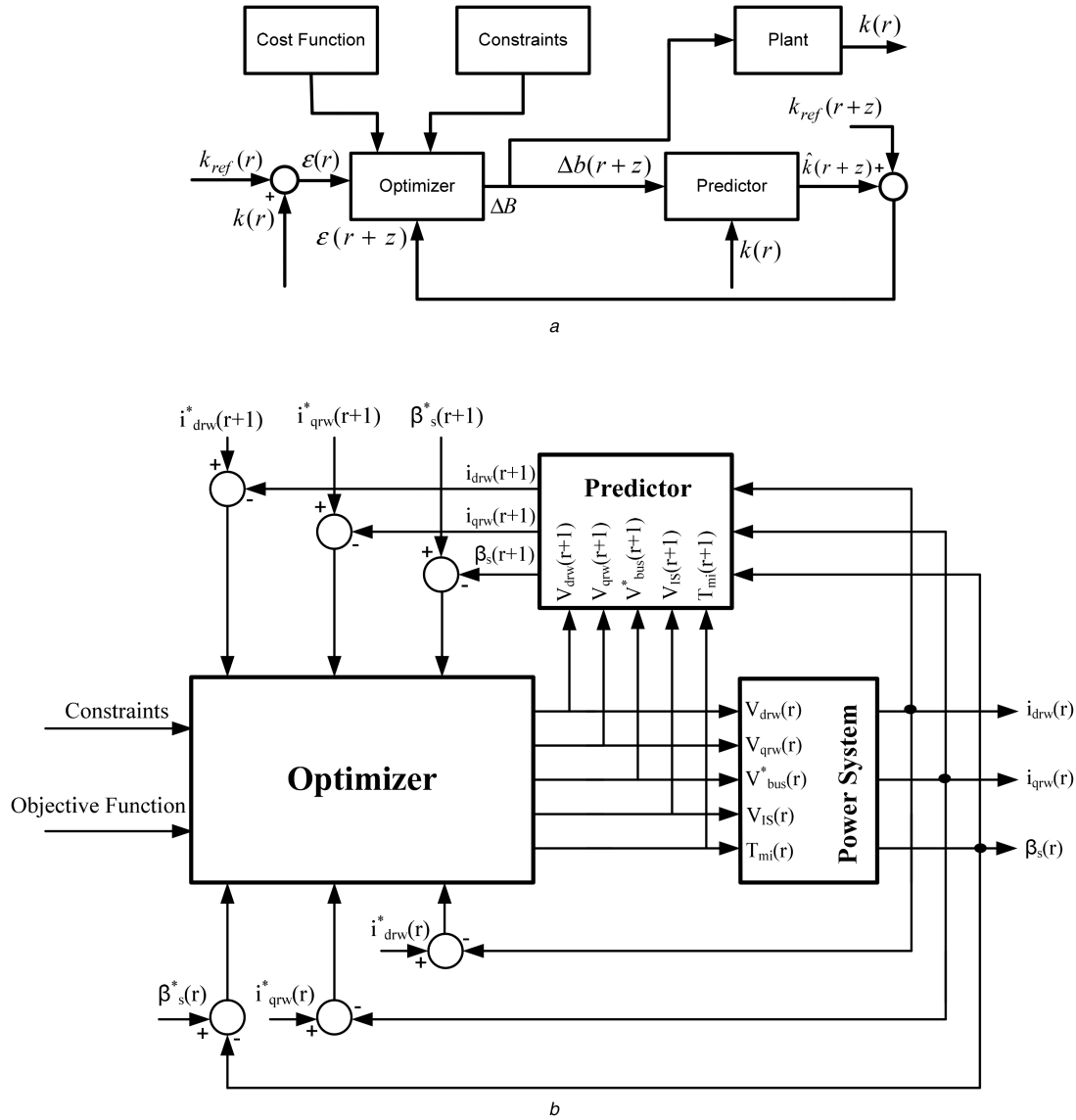


**Fig. 2** Block diagrams of the proposed model predictive control strategy

(a) Controller structure of the MPC.

(b) Block diagram of the proposed strategy

- Limitation on the amplitude and variations of the input.
- Limitation on the state variables.
- Limitation on the output variables.

These constraints can be mathematically described as

$$\begin{cases} b_{\min} \leq b(r+z) \leq b_{\max}, \Delta b_{\min} \leq \Delta b(r+z) \leq \Delta b_{\max} \\ x_{\min} \leq x(r+z) \leq x_{\max}, \Delta x_{\min} \leq \Delta x(r+z) \leq \Delta x_{\max} \\ k_{\min} \leq k(r+z) \leq k_{\max}, \Delta k_{\min} \leq \Delta k(r+z) \leq \Delta k_{\max} \end{cases} \quad (15)$$

Furthermore, a vector with the length of  $m_b$  having a forward transmission is used to control the future signals in MPC. This forward transmission matrix is defined as:

$$\Delta B = [\Delta b(r), \dots, \Delta b(r+z), \dots, \Delta b(r+m_b-1)] \quad (16)$$

### 3.2 Modelling the MPC using Laguerre functions

There is a challenging problem related to predictive control which has limited its application, and it is the computational burden in

online implementation of this controller. As a result, in the systems having low sampling times or complicated dynamics, the predictive control is faced with a huge number of decision variables leading to the deceleration of the real-time implementation. An applicable alternative for reducing the computational effort is the use of functional MPC (FMPC). In FMPC, for the selection of appropriate paths, the linear combination of the system's future inputs is considered as one or more basic functions. The functions used for modelling of the input path are named the Laguerre functions [28]. In these functions, by parameterising the series of control signals, the number of constraints in the prediction horizon, and consequently, the number of parameters considered at each stage can be decreased, and the computational burden of this controller in large-scale systems is lowered. The Laguerre functions are a set of discrete functions with orthogonal basis, which their Z-transform is represented by

$$\Gamma_g = \frac{\sqrt{1-b^2}}{z-b} \left( \frac{z^{-1}-b}{1-bz^{-1}} \right)^{g-1}, 0 \leq b \leq 1 \quad (17)$$

$$F_{\text{fit}}(r) = \sum_{z=1}^{m_a} G_z (k'(r+z) - k_{\text{ref}}(r+z))^2 + \sum_{z=1}^{m_b} S_z \Delta b(r+z)^2, \quad (14)$$

In this transform,  $b$  is the pole of the power system; if  $0 < b < 1$ , the system will be stable. Now, each input control signal can be described using the Laguerre functions as

$$\Delta b(r+z) \simeq \sum_{g=1}^m a_g \cdot f_g(z) \quad (18)$$

In (18),  $f_g$  is the transposed form of the Laguerre functions defined in (17), and  $a_g$  is named the parameter vector. In practical applications, the value of  $m$  is considered to be  $< 10$ . Choosing larger values for  $m$  will increase the input paths prediction for the Laguerre functions.

### 3.3 Exponentially weighted MPC

Closed-loop performance of MPC depends on the length of the prediction horizon. Generally, by increasing the magnitude of prediction horizon, the closed-loop performance will be improved. However, practically, selection of large prediction horizon is limited by numerical issues, particularly in the process with a high sampling rate. One approach to overcome this drawback is to use exponential data weighting in MPC:

$$\begin{cases} \Delta \hat{B}^T = [\rho^{-0} \Delta b(r), \dots, \rho^{-(m_b-1)} \Delta b(r+m_b-1)] \\ \hat{X}^T = [\rho^{-1} x(r+1), \dots, \rho^{-m_a} x(r+m_a)] \\ \hat{K}^T = [\rho^{-1} k(r+1), \dots, \rho^{-m_a} k(r+m_a)] \end{cases} \quad (19)$$

where the symbol  $\rho$  has been used for representing the adjustment of parameters in exponential weight. The value of  $\rho$  is chosen to be  $> 1$ . Therefore, the new equations of the utilised model in the state space can be explained as

$$\begin{cases} \hat{x}(r+1) = \hat{F}\hat{x}(r) + \hat{G}\Delta \hat{b}(r) \\ \hat{k}(r) = \hat{P}\hat{x}(r) \end{cases} \quad (20)$$

Substituting the following relations in (20) results in the new objective function as (22):

$$\hat{F} = \frac{F}{\rho}, \quad \hat{G} = \frac{G}{\rho}, \quad \hat{P} = \frac{P}{\rho} \quad (21)$$

$$\begin{aligned} \hat{F}_{\text{fit}}(r) = & \sum_{z=1}^{m_a} G_z (\hat{k}(r+z) - k_{\text{ref}}(r+z))^2 \\ & + \sum_{z=1}^{m_b} S_z \Delta \hat{b}(r+z)^2 \end{aligned} \quad (22)$$

Also, the constraints of (15) are modified to

$$\begin{cases} \rho^{-z} b_{\min} \leq \hat{b}(r+z) \leq \rho^{-z} b_{\max} \\ \rho^{-z} \Delta b_{\min} \leq \Delta \hat{b}(r+z) \leq \rho^{-z} \Delta b_{\max} \\ \rho^{-z} x_{\min} \leq \hat{x}(r+z) \leq \rho^{-z} x_{\max} \\ \rho^{-z} \Delta a_{\min} \leq \Delta \hat{x}(r+z) \leq \rho^{-z} \Delta x_{\max} \\ \rho^{-z} k_{\min} \leq \hat{k}(r+z) \leq \rho^{-z} k_{\max} \\ \rho^{-z} \Delta k_{\min} \leq \rho^{-z} \Delta \hat{k}(r+z) \leq \rho^{-z} \Delta k_{\max} \end{cases} \quad (23)$$

After solving (23), the input path should be rewritten as

$$\Delta B^T = [b^0 \Delta \hat{b}(r), \dots, b^{(m_b-1)} \Delta \hat{b}(r+z), \dots, \Delta b(r+m_b-1)] \quad (24)$$

Briefly, the sequence of solving the problem of functional predictive control can be followed as the following stages:

- Assigning a proper value for  $\rho$ .

- Substituting the matrices  $(F, G, P)$  and the variables  $(B, X, K)$  in (21) and (22).
- Applying the constraints in the objective function according to the characteristics of the problem using (23) and (24).
- Implementing the optimisation procedure for the objective function based on the Laguerre functions, and calculating the coefficients of this function.
- Processing the input control signals chosen by the Laguerre functions using (18).
- Sorting the inputs according to (24), and applying it to the considered system.

The functional MPC differs from the classical MPC in some aspects. The Laguerre function and the exponentially weights represented in (17) and (18) are employed to produce the initial control input sequence  $\Delta \hat{b}(r+z)$  in the case of functional MPC. Then, by minimising the cost function  $\hat{F}_{\text{fit}}(r)$  described by (22) the optimal control trajectory is achieved by means of the initial control input sequence. The computational burden to acquire the optimal control trajectory is reduced employing the initial control input sequence with suitable weighting factors,  $G_k$  and  $S_k$ . Whereas, in the case of classical MPC, minimising the cost function  $F_{\text{fit}}(r)$  described in (14) results in the optimal control trajectory  $\Delta b(r+z)$  directly. To minimise the cost function  $F_{\text{fit}}(r)$  in this case, more calculations are required to obtain the optimal control trajectory.

### 3.4 Adaptation of the presented strategy for the system under study

In this section, for implementation of the predictive strategy in the case study, it is required the relations of this strategy to be adapted with the power system model. Therefore, the system's dynamic equations including the equations of synchronous generators, wind farms, and static compensators must be determined in the state space. The state space equations are regarded as (25), in which  $X$  is the vector of the system states

$$\begin{cases} \dot{X} = AX + BU + ER \\ Y = CX + DU \end{cases} \quad (25)$$

In (25),  $D$  equals to zero, the input vector of the predictive control is  $U = [V_{drw}, V_{grw}, V_{bus}^*, V_{Is}, T_{mi}]^T$ ,  $Y = [i_{drw}, i_{grw}, \beta_s]^T$  is the regulation output,  $R = [V_{dsw}, V_{qsw}, V_{bus}]^T$  is considered as the disturbance vector and  $X$  is defined as follows:

$$\begin{cases} X = [X_{SG}, X_{RSC}, X_{STATCOM}]^T \\ X_{SG} = [E'_{di}, E'_{qi}, \delta_i, \omega_i] \\ X_{RSC} = [i_{dsw}, i_{qsw}, i_{drw}, i_{grw}] \\ X_{STATCOM} = [i_{ds}, i_{qs}, V_{dcs}, \beta_s] \end{cases} \quad (26)$$

To refine the resulted solution of the predictive control, the existing constraints must be defined in an allowed range. In this study, the constraints are defined as follows:

- Controlling the active and reactive powers of the DFIG for the sake of selecting appropriate reference vectors for the RSC by considering  $(V_{drw\_min} \leq V_{drw} \leq V_{drw\_max}, V_{grw\_min} \leq V_{grw} \leq V_{grw\_max})$ .
- Controlling the line power control by damping controller in order to provide proper signals for inverter switching in STSTCOM with a view to constraint  $(V_{Is\_min} \leq V_{Is} \leq V_{Is\_max})$ .

In total, the minimum and maximum values of the above descriptions for applying the constraints are as follows:

$$\begin{bmatrix} v_{drw\_min} \\ v_{grw\_min} \\ V_{Is\_min} \\ V_{Ri\_min} \end{bmatrix} = 0 \leq u \leq 1 = \begin{bmatrix} v_{drw\_max} \\ v_{grw\_max} \\ V_{Is\_max} \\ V_{Ri\_max} \end{bmatrix} \quad (27)$$

Consideration of constraints for the control signals increases the simulation time. However, the limitations on the state vectors are not faced with this problem. Hence, in this study, the limitations on the state vectors are regarded as follows (28):

$$\begin{bmatrix} i_{drw\_min} \\ i_{grw\_min} \\ \beta_{S\_min} \end{bmatrix} = \begin{bmatrix} 0 \\ 0 \\ 0 \end{bmatrix} \leq x \leq \begin{bmatrix} 3 \\ 7 \\ 0.7 \end{bmatrix} = \begin{bmatrix} i_{drw\_max} \\ i_{grw\_max} \\ \beta_{S\_max} \end{bmatrix} \quad (28)$$

Also, the parameters of the predictive control strategy used in the simulations have been considered as:  $m_b = 4$ ,  $m_a = 200$ ,  $\rho = 1.02$ ,  $m = 3$ ,  $b = 0.21$ . Also, the coefficient values of the weighting matrices have been selected as:  $G = 0.14 \times I_{mb \times mb}$ ,  $S = 1 \times I_{ma \times ma}$ , respectively. The sampling time for the predictive controller is assumed as 0.02 s. Predictive controller parameters have been chosen based on try and error. To understand more of the proposed method, a block diagram of the control loop is shown in Fig. 2B.

### 3.5 Objective function optimisation

In this section, an objective function based on the eigenvalue is used to optimise parameters of damping controller [25]. In this objective function, the real parts and the damping ratio of non-damping modes are formulated as follows:

$$\begin{aligned} \min J(K_G, T_G) &= w_1 \sum_{i=1}^N \sum_{\zeta_i \leq \zeta_0} (\zeta_0 - \zeta_{i,k})^2 \\ &+ w_2 \sum_{k=1}^N \sum_{\sigma_i \leq \sigma_0} (\sigma_0 - \sigma_{i,k})^2 \end{aligned} \quad (29)$$

Subject to:

$$\begin{aligned} K_{G_{min}} &\leq K_G \leq K_{G_{max}} \\ T_{G_{min}} &\leq T_G \leq T_{G_{max}} \end{aligned}$$

where  $\zeta_{ik}$  and  $\sigma_{ik}$  are related to the damping ratio and real part of  $i$ th eigenvalue from  $k$ th operating point;  $\sigma_0$  and  $\zeta_0$  are the minimum of real part and damping ratio, respectively;  $K_G$  and  $T_G$  are gains and constants of damping controllers, respectively; and  $w_1$  and  $w_2$  are weight values. In this paper,  $\sigma_0$  and  $\zeta_0$  are considered as  $-1$  and  $0.8$ , respectively. The following equation is used to find weight coefficients owing to their importance in damping oscillations

$$\begin{aligned} w_1 &= 1 - \text{error}_1 \\ w_2 &= 1 - \text{error}_2 \end{aligned} \quad (30)$$

$$\begin{aligned} \text{error} &= (\zeta_0 - \zeta_{i,k}) \zeta_{i,k} \\ \text{error} &= (\sigma_0 - \sigma_{i,k}) \zeta_{i,k} \end{aligned} \quad (31)$$

**3.5.1 Firefly algorithm:** To optimise the proposed objective function, the firefly algorithm is used. This algorithm is inspired by the blinking behaviour of firefly for self-protection or taking bait [29]. In summary it can be said that firefly  $d$  which has more glitter can absorb other  $c$  fireflies according to following relation:

$$x_{d+1} = x_d + \beta_t e^{-\rho \frac{d_c}{\rho}} (x_d - x_c) + \alpha_t (\text{rand} - 0.5)$$

where  $\alpha_t$  is a random parameter,  $\beta_t$  reflects the attractiveness of light source;  $\rho_{dc}$  is the distance between two fireflies in situations  $x_c$  and  $x_d$ , and  $\chi$  is determined according to the degree of the

attractiveness and is very useful in convergence. The distance between two fireflies can be described as follows:

$$\rho_{dc} = \sqrt{\sum_{j=1}^s (x_{d,j} - x_{c,j})^2} \quad (33)$$

$x_c$  and  $x_d$  include proportional integral (PI) controller parameters for RSC and STATCOM which are defined as the following vector:

$$\begin{aligned} x_d &= [Z_{q1}, Z_{q2}, Z_{q3}, Z_{i1}, Z_{i2}, Z_{i3}] \\ x_c &= [K_a, K_I, K_{Damp}, T_a, T_1, T_2, T_3, T_4] \end{aligned}$$

Steps for implementing the firefly algorithm to solve optimisation problem are shown in Fig. 3.

Optimal results of control parameters for STATCOM and RSC are shown in Table 1 in the Appendix.

## 4 Simulation results in three-machine power system

In this section, the simulation results for the three-machine power system are evaluated. Considering the single line diagram of this system which is shown in Fig. 4, a wind farm consisting of four 5 MW wind turbines based on DFIG in each unit and a 5 MVAR parallel STATCOM compensator is used.

### 4.1 Modal analysis and design of damping controller

In this section, initial points of the system in Table 2 are reported first. Then the results of modal analysis for each part of system are reported in Table 3. Considering this table, it can be seen that the  $\lambda_{19,20}$  and  $\lambda_{21,22}$  modes have the lowest damping ratio rather than other modes. These modes are related to rotor angle deviation  $\Delta\delta_{12}$  and  $\Delta\delta_{13}$ , respectively. Therefore they have been used for designing the damping controller for STATCOM in the three-machine power system. Damping controller input in this system is the flowing power of the line between the wind farm and power system, which is shown in Fig. 4.

### 4.2 Time domain simulation

In this section, by implementing a three-phase fault in bus 10 of the test system in Fig. 4, simulation results are evaluated in four different scenarios. This fault is implemented at 1 s and after 0.2 s is cleared.

**4.2.1 Scenario I:** In this scenario, the wind speed for wind units 1 and 2, is increased from 11 to 12 m/s and their rotor speed in super-synchronous mode was 1.09 p.u. Meanwhile, the wind speed for units 3 and 4 is decreased from 11 to 10 m/s and their rotor speed in synchronous mode was 1 p.u. In Fig. 5A rotor angle deviation of  $\Delta\delta_{12}$  is illustrated. In Figs. 5B and C the reactive power of STATCOM and common bus voltage is illustrated, respectively. Also, in Fig. 5D the active power response for wind unit 1 under wind speed changing is illustrated.

**4.2.2 Scenario II:** In this scenario, the wind speed for wind units 1 and 2 is increased from 11 to 12 m/s and their rotor speed in super-synchronous mode was 1.09 p.u. Meanwhile, the wind speed for units 3 and 4 is decreased from 11 to 8.5 m/s and their rotor speed in sub-synchronous mode was 0.729 p.u. In Figs. 6A) and B) the STATCOM reactive power and SG<sub>1</sub> terminal voltage are illustrated, respectively. In Figs. 6C and D) the reactive power and DC link capacitor voltage for wind unit 3 are illustrated, respectively.

**4.2.3 Scenario III:** In this scenario, the simulation results are evaluated by sever arbitrary changing of wind for wind units 1–2 and 3–4. The oscillation pattern for wind units is shown in Fig. 7A. The active power of wind unit 1 is illustrated in Fig. 7B. In

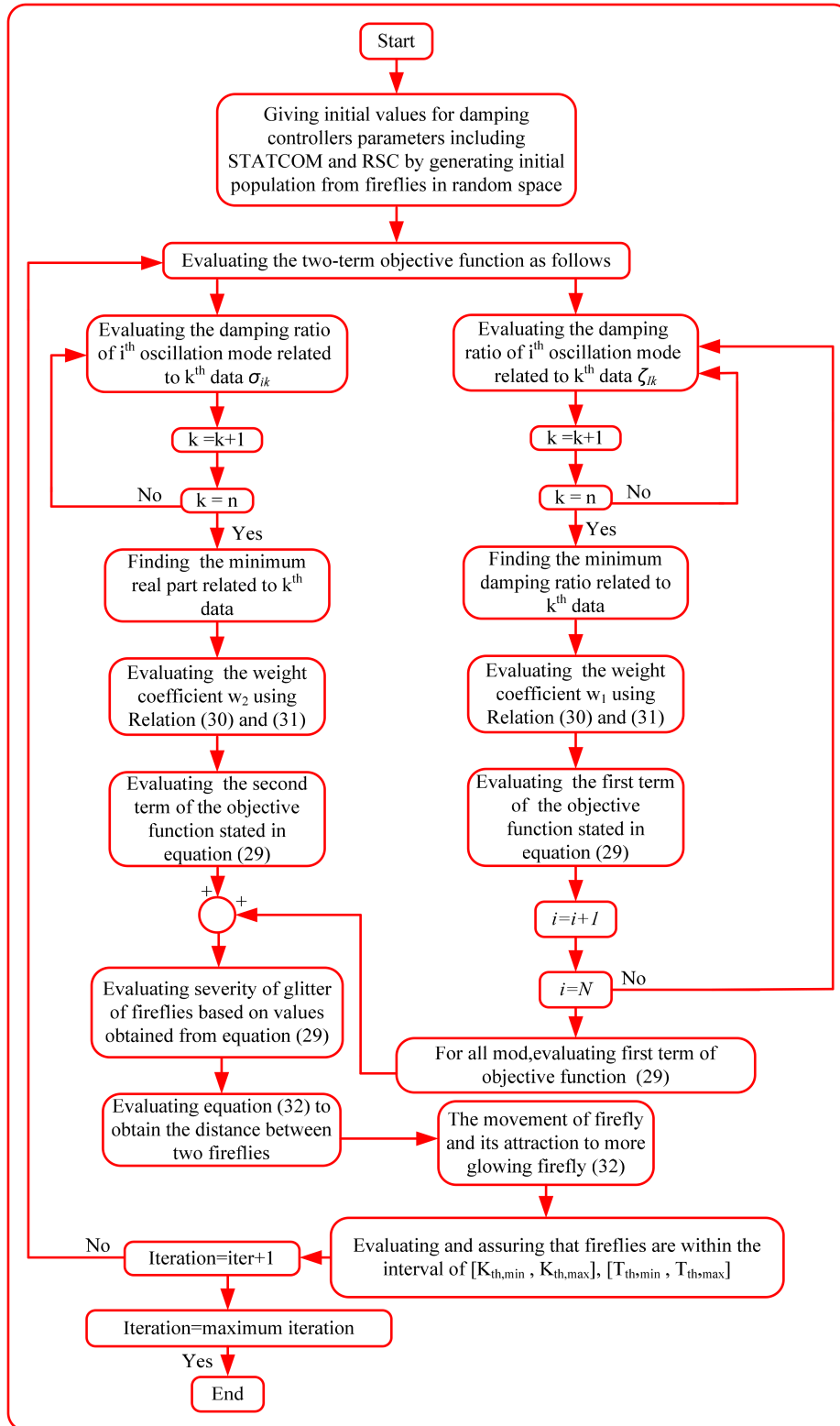


Fig. 3 Flowchart of the firefly algorithm

Figs. 7C and D the input control signal ( $V_{IS}$ ) and STATCOM reactive power are illustrated, respectively.

**4.2.4 Scenario IV:** In this scenario with implementing a two-phase-to-ground fault at 1 s between bus 10 and 11, simulation results are evaluated. Fault duration was 0.1 s. The wind speed for wind units was considered the same as in Scenario III. With this difference by implementing a delay in damping controller input, response changing is illustrated in Fig. 8. In Fig. 8A, the reactive power of wind unit 1 is illustrated. In Figs. 8B–D the active power of wind unit 3 and STATCOM and PCC bus voltage for the 200 ms delay is illustrated, respectively. As it can be seen from these

figures, even with the existence of delay, oscillation damping by the proposed controller is robust and fine.

Finally, in Fig. 8E the input control signal of STATCOM and in Fig. 8F the input control signal of RSC are illustrated.

In all scenarios, it can be seen that the proposed controller, in comparison with the other controllers in the paper, has a finer performance in overshoot, undershoot and settling time.

### 4.3 Computational aspects of the method

In this section, the performance of FMPC and MPC controllers in terms of computational time and objective functions are evaluated.

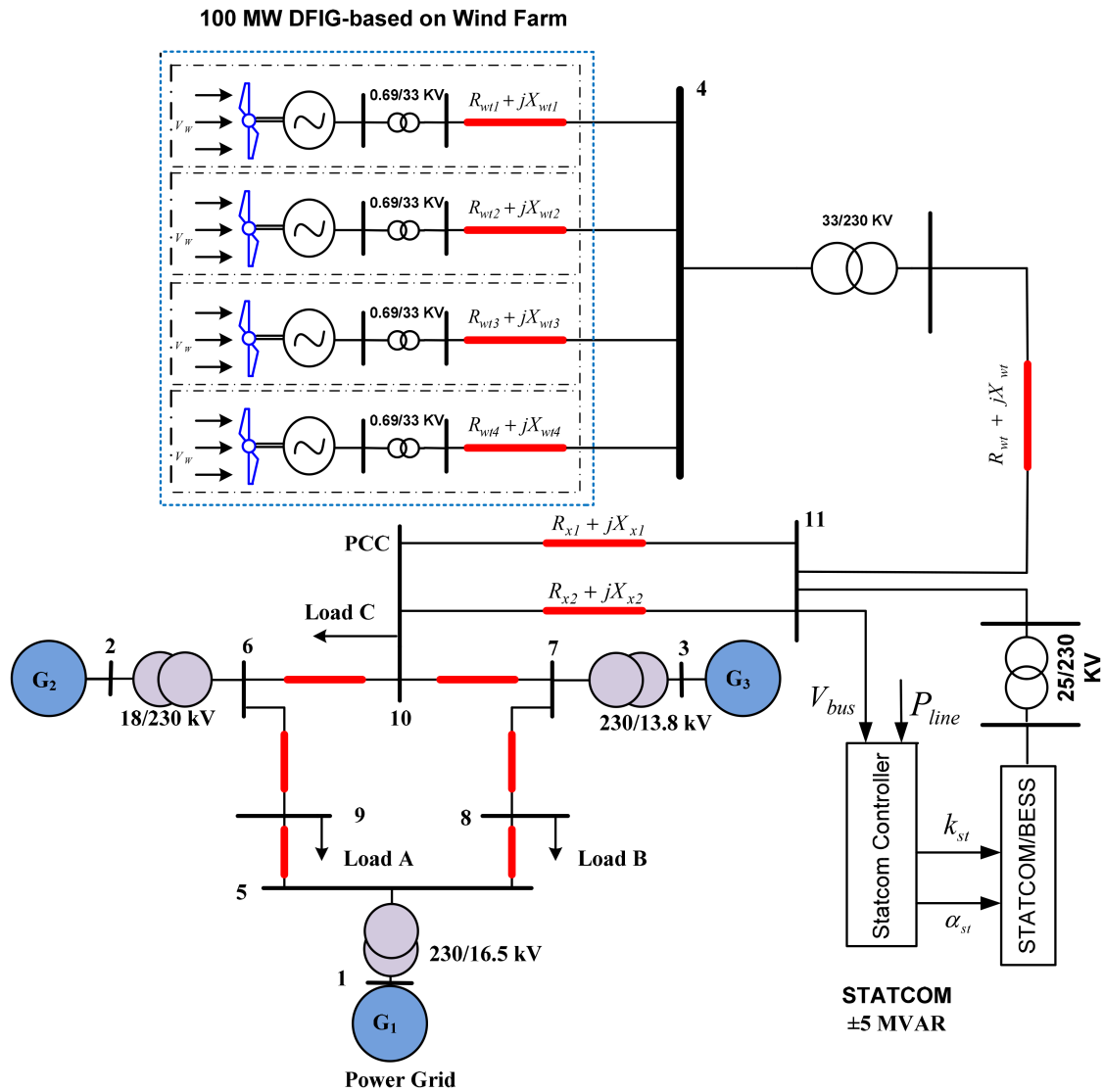


Fig. 4 Single line diagram of three-machine nine-bus power system

Table 2 Initial points for each wind turbine in three-machine power system

V, p.u.	Wind speed, m/s	Q, MVAR	P, MW	Ω, p.u.
1	11	2.4215	5	1

As seen in Table 4, the value of objective function for FMPC is far less than MPC for both power systems. Since the objective function is defined as the difference between input and output signals, it can be concluded that the least value in this case represents the optimal performance of the controllers. Given that the unknown variables in FMPC are 20 times less than MPC, therefore the computational time for each iteration of FMPC is much less than that of MPC as shown in Table 4. This reduction in the computational time can be considered as a benefit for the FMPC controller.

## 5 Conclusion

In this study, small signal stability for a three-machine power system, in the presence of wind units and STATCOM by predictive control was investigated. To use the presented MPC, at the first state space model of the under-study system was extracted and then, the connection approach of the power system with the predictive control was determined in a block diagram. MPC was used for controlling the power of DFIGs and to improve the inter-area oscillation by predictive damping control in STATCOM. To reduce the computational burden in the proposed MPC, Laguerre functions were used for precise tracking of input paths and exponential data weighing was used for reducing the sampling

time. Simulation results in four different scenarios of uncertainties caused by wind change, three-phase and two-phase faults, and also existence of time delay in input of the damping controller was challenged. Moreover, it was demonstrated that the proposed MPC has a more robust performance in comparison with the conventional MPC or PI controller. Finally, a comparison of time between the proposed predictive control and conventional MPC was performed and it was demonstrated that the time of conventional MPC is far more than the predictive control which uses Laguerre functions.

**Table 3** Modal analysis results for the most critical eigenvalue in three-machine power system

		Without damping controller for STATCOM		With damping controller for STATCOM	
Mode type		Eigenvalues	$\zeta$	Eigenvalues	$\zeta$
$\lambda_{2,1}$	$X_{SG-ELEC}$	$-1.959 \pm 7.203j$	0.2624	$-4.101 \pm 7.236j$	0.4930
$\lambda_{3,4}$		$-1.584 \pm 6.855j$	0.2251	$-4.291 \pm 7.103j$	0.5170
$\lambda_{6,5}$		$-1.789 \pm 7.122j$	0.2436	$-4.166 \pm 6.445j$	0.5428
$\lambda_{8,7}$		$-1.727 \pm 6.883j$	0.2433	$-4.201 \pm 6.994j$	0.5149
$\lambda_{9,10}$		$-1.662 \pm 6.344j$	0.2534	$-4.356 \pm 7.267j$	0.5141
$\lambda_{2,1}$		$-1.569 \pm 6.785j$	0.2252	$-4.114 \pm 7.598j$	0.4761
$\lambda_{11,12}$		$-1.654 \pm 7.465j$	0.2163	$-4/457 \pm 7.567j$	0.5075
$\lambda_{13,14}$		$-1.688 \pm 7.319j$	0.2247	$-4.228 \pm 7.496j$	0.4912
$\lambda_{15,16}$		$-1.577 \pm 6.167j$	0.2148	$-4.745 \pm 7.237j$	0.5483
$\lambda_{17,18}$		$-1.695 \pm 7.167j$	0.2301	$-4.993 \pm 7.761j$	0.5410
$\lambda_{19,20}$	$X_{SG-MECH}$	$-0.571 \pm 10.367j$	0.0549	$-3.146 \pm 7.255j$	0.3978
$\lambda_{21,22}$		$-0.493 \pm 10.577j$	0.04656	$-3.374 \pm 7.993j$	0.3889
$\lambda_{22,23}$	$X_{DFIG}$	$-2.457 \pm 7.798j$	0.3005	$-3.594 \pm 6.762j$	0.4693
$\lambda_{24,25}$		$-1.548 \pm 6.679j$	0.2257	$-4.478 \pm 7.549j$	0.5101
$\lambda_{26,27}$		$-1.789 \pm 7.694j$	0.2264	$-4.279 \pm 7.699j$	0.4857
$\lambda_{28,29}$		$-2.231 \pm 7.235j$	0.2946	$-4.159 \pm 6.574j$	0.5243
$\lambda_{30,31}$	$X_{STATCOM}$	$-2.447 \pm 7.862j$	0.2971	$-4.456 \pm 7.614j$	0.5050
$\lambda_{32,33}$		---	---	$-4.736 \pm 7/699j$	0.5239

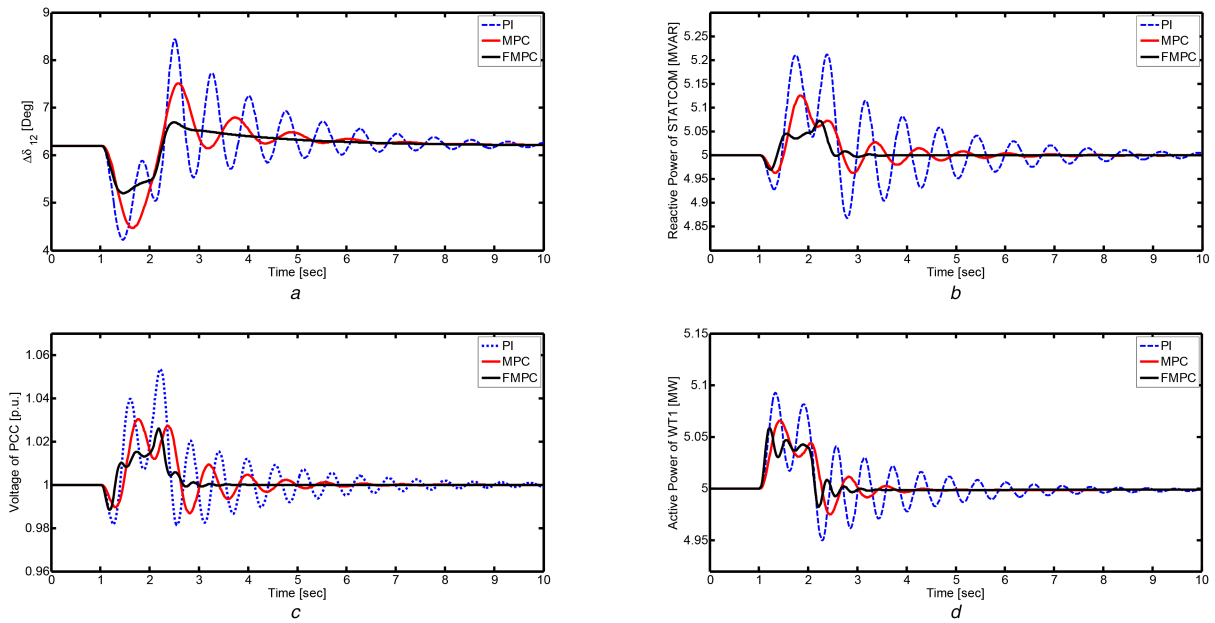


**Fig. 5** Response of time-domain simulation for scenario I

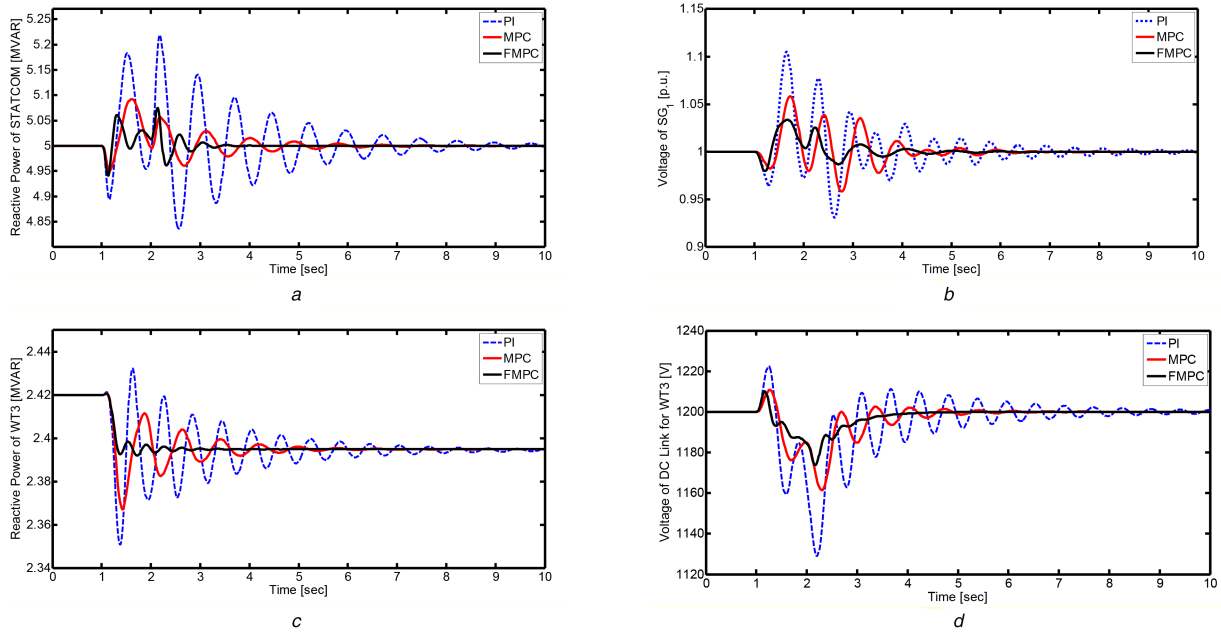


Fig. 6 Response of time-domain simulation for scenario II

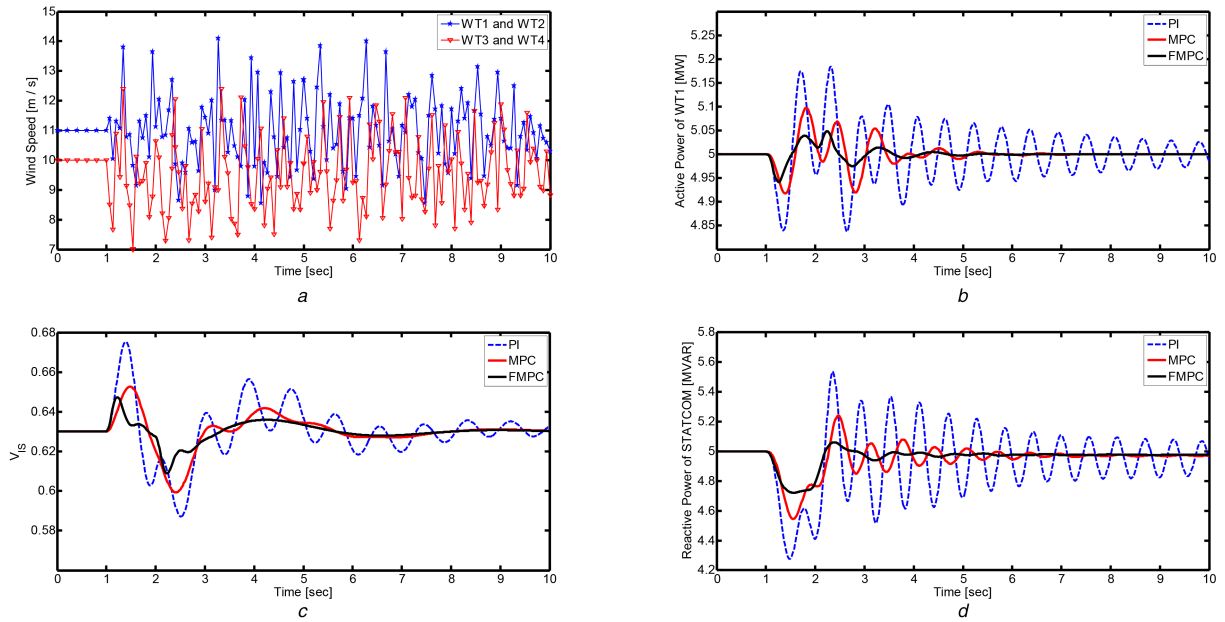


Fig. 7 Response of time-domain simulation for scenario III

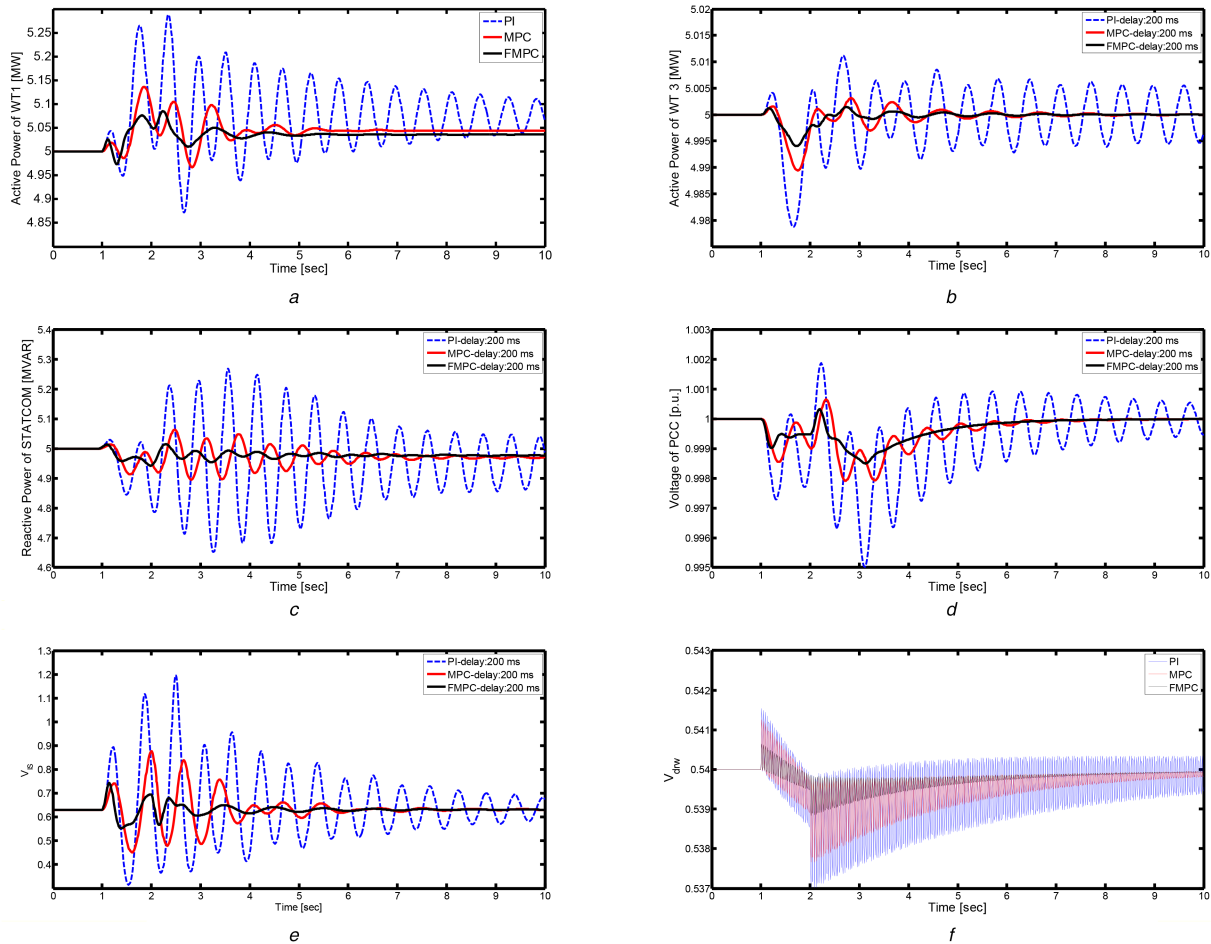


Fig. 8 Response of time-domain simulation for scenario IV

Table 4 Performance of the proposed controllers in terms of objective function and computational time

Scenarios	$m_a, m_b$		Computational time per iteration		Cost function	
	MPC	FMPC	Method		MPC	FMPC
			MPC	FMPC		
I	200, 80	200, 4	3.71	0.37	0.153	0.131
II	200, 80	200, 4	3.44	0.53	0.148	0.133
III	200, 80	200, 4	3.21	0.35	0.151	0.144
IV	200, 80	200, 4	3.25	0.41	0.153	0.132

## 6 References

- [1] Muljadi, E, Singh, M., Gevorgian, V.: 'Doubly fed induction generator in an offshore wind power plant operated at rated V/Hz', *IEEE Trans. Ind. Appl.*, 2013, **49**, (5), pp. 2197–2205
- [2] Yan, J., Lin, H., Feng, Y., *et al.*: 'Improved sliding mode model reference adaptive system speed observer for fuzzy control of direct-drive permanent magnet synchronous generator wind power generation system', *IET Renew. Power Gener.*, 2013, **7**, (1), pp. 28–35
- [3] Ghanizadeh, R., shendi, A.J., Ebadian, M., *et al.*: 'A multi-objective HBMO-based new FC-MCR compensator for damping of power system oscillations', *J. Oper. Autom. Power Eng.*, 2013, **1**, (2), pp. 110–123
- [4] Muyeen, S.M., Hasanien, H.M., Durra, A.A.: 'Transient stability enhancement of wind farms connected to a multi-machine power system by using an adaptive ANN-controlled SMES', *Energy Convers. Manage.*, 2014, **78**, (1), pp. 412–420
- [5] Hasanien, H.M.: 'Shuffled frog leaping algorithm-based static synchronous compensator for transient stability improvement of a grid-connected wind farm', *IET Renew. Power Gener.*, 2014, **8**, (6), pp. 722–730
- [6] Wang, L., Truong, D.N.: 'Stability enhancement of a power system with a PMSG-based and a DFIG-based offshore wind farm using a SVC with an adaptive-network-based fuzzy inference system', *IEEE Trans. Ind. Electron.*, 2013, **60**, (7), pp. 2799–2807
- [7] Wang, L., Truong, D.N.: 'Dynamic stability improvement of four parallel-operated PMSG-based offshore wind turbine generators fed to a power system using a STATCOM', *IEEE Trans. Power Deliv.*, 2013, **28**, (1), pp. 111–119

- [8] Wang, L., Truong, D.N.: 'Stability enhancement of DFIG-based offshore wind farm fed to a multi-machine system using a STATCOM', *IEEE Trans. Power Syst.*, 2013, **28**, (3), pp. 2882–2889
- [9] Hui, L., Shengquan, L., Haiting, J., *et al.*: 'Damping control strategies of inter-area low-frequency oscillation for DFIG-based wind farms integrated into a power system', *Int. J. Electr. Power Energy Syst.*, 2014, **61**, (10), pp. 279–287
- [10] Fan, L.L., Yin, H.P., Miao, Z.X.: 'On active/reactive power modulation of DFIG-based wind generation for interarea oscillation damping', *IEEE Trans. Energy Convers.*, 2011, **26**, (2), pp. 513–521
- [11] Qiao, W., Harley, R.G., Venayagamoorthy, G.K.: 'Coordinated reactive power control of a large wind farm and a STATCOM using heuristic dynamic programming', *IEEE Trans. Energy Convers.*, 2009, **24**, (2), pp. 493–503
- [12] Vittal, E., O'Malley, M., Keane, A.: 'Rotor angle stability with high penetrations of wind generation', *IEEE Trans. Power Syst.*, 2012, **27**, (1), pp. 353–362
- [13] Bijami, E., Askari, M., Farsangi, M.: 'Design of stabilising signals for power system damping using generalized predictive control optimized by a new hybrid shuffled frog leaping algorithm', *IET Gener. Transm. Distrib.*, 2012, **6**, (10), pp. 1036–1045
- [14] Darabian, M., Jalilvand, A., Azari, M.: 'Power system stability enhancement in the presence of renewable energy resources and HVDC lines based on predictive control strategy', *Int. J. Electr. Power Energy Syst.*, 2016, **80**, (9), pp. 363–373
- [15] Azad, S.P., Irvani, R., Tate, J.E.: 'Damping inter-area oscillations based on a model predictive control (MPC) HVDC supplementary controller', *IEEE Trans. Power Syst.*, 2013, **28**, (3), pp. 3174–3183
- [16] Han, J., Solanki, S.K., Solanki, J.: 'Coordinated predictive control of a wind/Battery microgrid system', *IEEE J. Emerging Sel. Top. Power Electron.*, 2013, **1**, (4), pp. 296–305
- [17] Yang, J., Zheng, W.X.: 'Offset-free nonlinear MPC for mismatched disturbance attenuation with application to a static var compensator', *IEEE Trans. Circuits Syst. II, Express Briefs*, 2014, **61**, (1), pp. 49–53
- [18] Ford, J.J., Ledwich, G., Dong, Z.Y.: 'Efficient and robust model predictive control for first swing transient stability of power systems using flexible AC transmission systems devices', *IET Gener. Transm. Distrib.*, 2008, **2**, (5), pp. 731–742
- [19] Zheng, Y., Li, S., Li, N.: 'Distributed model predictive control over network information exchange for large-scale systems', *Control Eng. Pract.*, 2011, **19**, (7), pp. 757–769
- [20] Hadjiski, M., Asenov, V.: 'Predictive functional control using a blending approach', *Cybern. Inf. Technol.*, 2005, **5**, (2), pp. 32–41

- [21] Liu, H., Li, S.: 'Speed control for PMSM servo system using predictive functional control and extended state observer', *IEEE Trans. Ind. Electron.*, 2012, **59**, (2), pp. 1171–1183
- [22] Padiyar, K.R.: '*Power system dynamics-Stability and Control*' (BS Publications, Hyderabad, India, 2002)
- [23] Hany, H., Muyeen, M.: 'Design optimization of controller parameters used in variable speed wind energy conversion system by genetic algorithms', *IEEE Trans. Sustain. Energy*, 2012, **3**, (2), pp. 200–208
- [24] Yang, L., Xu, Z., Ostergaard, J., *et al.*: 'Oscillatory stability and eigenvalue sensitivity analysis of a DFIG wind turbine system', *IEEE Trans. Energy Convers.*, 2011, **26**, (1), pp. 328–339
- [25] Shayeghi, H., Shayanfar, H., Jalilzadeh, S., *et al.*: 'Multi-machine power system stabilizers design using chaotic optimization algorithm', *Energy Convers. Manage.*, 2010, **51**, (7), pp. 1572–1580
- [26] Zong, Y., Kullmann, D., Thavlov, A., *et al.*: 'Application of model predictive control for active load management in a distributed power system with high wind penetration', *IEEE Trans. Smart Grid*, 2012, **3**, (2), pp. 1055–1062
- [27] Evans, A.M., Cannon, M., Kouvaritakis, B.: 'Robust MPC tower damping for variable speed wind turbines', *IEEE Trans. Control Syst. Technol.*, 2015, **23**, (1), pp. 290–296
- [28] Palomo, G.V., Rossiter, J.A.: 'Novel programmable logic controller implementation of a predictive controller based on Laguerre functions and multi-parametric solutions', *IET Control Theory Applic.*, 2012, **6**, (8), pp. 1003–1014
- [29] Kavousi-Fard, A., Niknamand, T., Baziar, A.: 'A novel multi-objective self-adaptive modified firefly algorithm for optimal operation management of stochastic DFR strategy', *Int. Trans. Electr. Energy Syst.*, 2015, **25**, (6), pp. 976–993

## 7 Appendix

See Table 1.

**Table 1a** Employed system parameters

The optimal parameters of the system under study															
parameters	$Z_{q1}$	$Z_{q2}$	$Z_{q3}$	$Z_{i1}$	$Z_{i2}$	$Z_{i3}$	$K_a$	$K_I$	$K_{Damp}$	$T_a$	$T_1$	$T_1$	$T_2$	$T_3$	$T_4$
without optimisation	8.2	7.4	7.2	2.1	2.37	2.83	17.7	14.2	12.8	0.25	0.43	0.17	0.36	0.29	0.22
with optimisation	15.6	17.1	12.5	6.9	7.5	5.6	22.87	20.19	18.67	0.61	0.72	0.54	0.68	0.45	0.51

**Table 1b**

DFIG-based wind turbine (100 MW)									
$P = 25$ MW	$V = 0.69$ kV	$R_s = 0.042$ pu	$R_r = 0.005$ pu	$C_{dc} = 0.01$ F	$L_{mm} = 2.9$ pu	$L_{rr} = 3.056$ pu	$L_{ss} = 3.071$ pu	$X_{lg} = 0.55$ pu	
$K_t = 0.5$ p.u.	$K_{tg} = 2.5$ p.u.	$L_{tg} = 0.93$ p.u.	$H_t = 0.05$ p.u.	$H_g = 10.2$ p.u.	$Z_{q1} = 15$	$Z_{i1} = 9.2$	$Z_{q2} = 8.6$	$Z_{i2} = 3.87$	
$Z_{q3} = 15$	$Z_{i3} = 9.2$	$Z_{bg} = 17.35$	$Z_{ig} = 10.43$	$Z_{pb} = 12$	$Z_{ib} = 8.53$	$\beta_{wt\_min} = 0^\circ$	$\beta_{wt\_max} = 30^\circ$	$Z_{b\beta} = 1.11$	
$d_1 = 0.22$	$d_2 = 116$	$d_3 = 0.954$	$d_4 = 0.18$	$d_5 = 0.955$	$d_6 = 6.161$	$d_7 = 11.89$	$d_8 = -12.95$	$d_9 = 0.088$	

**Table 1c**

STATCOM ( $\pm 50$ MVAR)					
$\beta_{s0} = 0.5$	$\beta_{smin} = 0$ (deg)	$\beta_{smax} = 0.7$ (deg)	$kn_{smin} = 0$ (deg)	$kn_{smax} = 0.6$ (deg)	$T_w = 10$

**Table 1d**

The optimal parameters of IEEE DC1A exciters								
Generators	$T_i$	$K_b$	$T_b$	$K_f$	$T_f$	$T_e$	$E_{fd\_max}$	$E_{fd\_min}$
1	0.031	4.2	0.07	0.035	1.05	0.27	5.3	-5.3
2	0.031	5.1	0.075	0.05	1.05	0.27	5.3	-5.3
3	0.031	7.9	0.06	0.05	1.02	0.25	5.1	-5.1

**Table 1e**

The optimal parameters of PSS									
Generators	$T_w$	$K_{DAMP}$	$T_1$	$T_1$	$T_2$	$T_3$	$T_4$	$V_{s\_max}$	$V_{s\_min}$
1	10	2	0.015	0.51	0.55	0.47	0.52	0.12	-0.12
2	10	2	0.015	0.53	0.55	0.47	0.55	0.12	-0.12
3	10	2.2	0.015	0.51	0.55	0.47	0.55	0.12	-0.12